Original Paper

Material-Driven Therapeutics to Establish a Penetrating Traumatic Brain Injury Rat Model and Implantation of a 3D-Printed Scaffold: Pre-Experimental Pilot Study

Meaghan E Harley-Troxell[1], PhD; Michelle Dennis[2], PhD; Madhu Dhar[1], PhD

[1]Tissue Engineering and Regenerative Medicine Lab, LACS, College of Veterinary Medicine, University of Tennessee at Knoxville, Knoxville, TN, United States

[2]Biomedical and Diagnostic Sciences Department, College of Veterinary Medicine, University of Tennessee at Knoxville, Knoxville, TN, United States

Corresponding Author:

Meaghan E Harley-Troxell, PhD
Tissue Engineering and Regenerative Medicine Lab, LACS, College of Veterinary Medicine
University of Tennessee at Knoxville
2407 River Drive
Knoxville, TN 37996
United States
Phone: 1 (865) 974-5703
Email: mharley-troxell@som.umaryland.edu

Related Articles:
Preprint (medRxiv): https://www.biorxiv.org/content/10.1101/2025.03.20.644358v1
Peer-Review Report by Firas Kobeissy (Reviewer EW): https://bio.jmirx.org/2026/1/e105277
Authors' Response to Peer-Review Reports: https://bio.jmirx.org/2026/1/e105278

Abstract

Background: Traumatic brain injuries (TBIs) are a leading cause of death and disability, with penetrating TBIs the most lethal form. While no TBI treatments currently exist, ongoing investigations are developing biomaterial scaffolds and cellular therapies to improve the poor outcomes of this disease.

Objective: This pilot study established a TBI rat model that maintains focal damage to the cerebral cortex while manually disrupting the blood-brain barrier (BBB). BBB-disrupting injuries require different management from others, allowing us to develop a specific, therapeutic treatment for this type of injury. We hypothesized that our method of BBB disruption would indicate behavioral, physical, and histological evidence of a TBI. Our TBI model will also create a cranial opening in which we can ensure surgical feasibility of implantation of a scaffold. We hypothesized that the implantation of a Food and Drug Administration–approved synthetic polymer, poly(lactic-co-glycolic) acid (PLGA), and a carbon-based nanomaterial, reduced graphene oxide (rGO), would not show evidence of foreign body rejection 30 days after surgery.

Methods: Sprague Dawley rats (N=4) underwent stereotaxic surgery with a 5-mm craniotomy. The dura and brain tissue were disrupted using a beaver blade. The PLGA/rGO scaffold was gently placed onto the brain tissue. Neurological function (including body condition, breathing, spontaneous behavior, handling reaction) was evaluated for the first 3 days, then weekly throughout the 30-day study. At 30 days, the brains were dissected, paraffin embedded, and sectioned for H&E and Prussian blue staining, and immunohistochemistry (IHC) using glial fibrillary acidic protein, neuronal nuclei (NeuN), von Willebrand factor, neurofilament light chain, ionized calcium-binding adapter molecule 1, and CD68 markers. Data were expressed as means and SDs, and 2-tailed *t* tests were used to determine statistical significance ($P \leq .05$).

Results: Neurological function assessments indicated no change in rat behavior and normal wound healing over the 30-day study. H&E and Prussian blue staining indicated mild leptomeningeal thickening and evidence of hemosiderin in 3 rats. One rat had foreign body giant cells and an abscess around the implanted material, with evidence of more severe leptomeningeal thickening and hemosiderin. IHC indicated normal anatomic structures with no changes in 5 of the 6 markers 30 days after surgery. NeuN significantly decreased in expression, from 9.65% to 4.56% in area, for all 4 rats ($P=.02$).

Conclusions: While there was no behavioral or symptomatic evidence of TBI, histology showed evidence of mild, focal TBI in 3 of the 4 rats and evidence of a foreign body response and a severe, focal TBI in 1 rat. This pilot study provides a basis for future studies to perform IHC at earlier time points to confirm additional biomarkers. Future studies will also implant a scaffold that is more mechanically aligned with the brain tissue to further evaluate the biocompatibility of graphene nanoparticles in brain tissue and the effectiveness of a therapeutic scaffold.

JMIRx Bio 2026;4:e75613; doi: 10.2196/75613

Keywords: penetrating traumatic brain injury; stereotaxic surgery; graphene; nerve tissue engineering; rat model

Introduction

Traumatic brain injuries (TBIs) are a leading cause of death and disability [1,2]. Annually in the United States, approximately 1.7 million people have a TBI event, resulting in 50,000 deaths [1]. Currently, it is estimated that 3.2 to 5.3 million people are living with a TBI-related disability [1]. Penetrating TBIs are the most lethal form, with a foreign object breaking through the skull, disrupting the blood-brain barrier (BBB), and damaging the brain tissue [3,4]. These are most often caused by accidents, including household firearm accidents, falls, and motor vehicle collisions [2-4]. The severity of the primary injury is worsened by circulating immune cells foreign to the local environment crossing the disrupted BBB, causing persistent inflammation and generation of reactive oxygen species that result in loss of neural tissue and damaged vasculature [1,2,5]. This damage results in severe clinical symptoms, including high cranial pressure and hemorrhage. While no treatments for TBI exist, management strategies include various neurosurgical interventions and pharmacological and nonpharmacological methods [2-4,6-8]. While surgical interventions may improve survival outcomes for severe TBIs, they come with increased risk of infection and longer recovery times and may not result in greater functional outcomes [3]. Currently, researchers are investigating tissue engineering and regenerative medicine strategies to develop biomaterial scaffolds and cellular therapies that may improve upon these poor outcomes [2,6,7,9].

Animals are a necessary preclinical step for translational research in the development of novel therapeutics and can help generate TBI solutions for both animal and human medicine [10]. While large animals such as pigs are important models for TBI, showing more complexity and gray and white matter ratios similar to those of human brains, using rodents such as rats or mice prior to large animal models is a crucial step [11,12]. Outside the advantages of low costs and easy handling, rats offer a high level of standardization and can be assessed for functional outcomes and the pathophysiology of cellular damage in a way that mimics the human brain [11]. Several preclinical models exist to mimic TBIs, including controlled cortical impact injury models, weight drop models, and penetrating ballistic-like models [13]. There are a wide range of TBIs, and while each model excels in representing a specific type of scenario, they do not consistently disrupt the BBB while maintaining controlled, focal damage to the cerebral cortex, as intended in this study [13,14]. Severe mechanical models often impact the brain as a whole, simulating concussion-like injuries alongside the penetrating impact and resulting in high levels of fatality [14]. Meanwhile, the penetrating ballistic-like model, while remaining focal, creates a deep cavity mimicking a combat setting. Adding to the available preclinical models to accurately represent the range of TBIs may alter how clinical care is managed and be useful in evaluating more specific, novel therapeutics [15].

Two oxidized derivatives of graphene nanoparticles, specifically reduced graphene oxide (rGO) and graphene oxide, have been investigated as nanocomposite components for nerve tissue engineering due to their elemental composition and topographic features, which influence their tunable mechanical properties and have a positive effect on cell growth [16,17]. Specifically, rGO can be engineered using a variety of 3D printing techniques to form scaffolds that attach, proliferate, and differentiate viable exogenous or endogenous stem and progenitor cells to aid in nerve repair and regeneration [17-19]. In particular, rGO features the unique property of electrical conductivity to improve functional nerve restoration [16,17,20]. While many studies have focused on graphene's potential in the peripheral nervous system, graphene and its derivatives have also shown to be a promising component for central nerve injuries [21-23]. Controversy surrounding rGO's biocompatibility has slowed its translation to clinical use. Numerous variables, such as surface functionalization, particle shape and size, dispersion, concentration, dosage, route of administration, and processing techniques, can all influence how cells respond to rGO [16,20,23-29]. Therefore, we must evaluate whether our specific rGO-containing construct is safe to use in this delicate tissue model.

For 3D printing, graphene-based nanoparticles are always blended with synthetic polymers, including polycaprolactone, polyurethane, polylactic acid, and poly(lactic-co-glycolic) acid (PLGA). PLGA is Food and Drug Administration approved for biomedical devices, primarily because of its tailored biodegradability (ie, its breakdown products, lactic and glycolic acids, are safely metabolized by the body). While PLGA is a Food and Drug Administration–approved and very well–characterized synthetic polymer, graphene's biocompatibility is highly variable depending on a variety of tunable physicochemical and mechanical properties [30]. Hence, it is important to evaluate the biocompatibility of a PLGA-rGO construct in vivo.

In this pilot study, we performed a craniotomy in rats to manually cut the BBB, managing the disruption to the brain tissue. This allowed us to assess the feasibility of our therapeutic scaffold implantation and the safety of the

biomaterial-tissue interaction between the brain tissue and our proposed scaffold containing PLGA and graphene. The use of stereotaxic surgical equipment and cranial landmarks allowed for a standardized injury capable of replication. We used a neurological assessment and immunohistochemistry (IHC) to identify whether disruption of the BBB was sufficient to model a TBI while identifying whether a foreign body reaction occurred with the implanted materials. For this study, we used a previously fabricated scaffold to evaluate the graphene's biocompatibility with the brain tissue. We hypothesized that the disruption of the BBB would cause behavioral, physical, and histological evidence of a TBI, whereas the implanted material would not show evidence of a foreign body rejection or chronic inflammation 30 days after surgery.

Methods

Biochemicals, Chemicals, and Disposables

All biochemicals, cell culture supplements, and disposable tissue culture supplies were purchased from Thermo Fisher Scientific unless otherwise noted.

Ethical Considerations

Sprague Dawley rats (Charles River Laboratories; N=4; male; aged 6 months) were acclimated prior to beginning procedures. All procedures were conducted in accordance with Public Health Service guidelines for the humane treatment of animals under approved protocols established through the University of Tennessee's Institutional Animal Care and Use Committee (protocol 2954-0623). The animals were housed in a 12-hour light and dark cycle with ad libitum food and water.

Surgical Procedure

Rats were anesthetized using inhalant isoflurane, and buprenorphine (0.05 mg/kg) was administered subcutaneously prior to surgery. The surgical area was shaved, and eye lubricant was applied. Under aseptic conditions, the rat was mounted onto the stereotaxic apparatus (Kopf Instruments) using a nose cone to maintain anesthesia throughout the procedure [7,31,32]. The dorsal and ventral adaptor was aligned to the –8 setting; the ear bars were aligned to the 7.5 setting on either side. The area was draped, and the scalp was cleaned using iodine prior to cutting a 1- to 2-cm longitudinal incision to expose the skull. The periosteum was gently teased back from the skull, and the area was cleaned using 95% ethanol. A handheld microdrill (Stoelting Co.) with a sterile 5-mm drill bit was used to create a craniotomy to the left of the sagittal suture, midway between the lambda and bregma landmarks. The dura mater was damaged by cutting the layer using forceps and a beaver blade. A 65:35 PLGA (Sigma-Aldrich) and 0.5% rGO (Cheap Tubes) scaffold from a previous study was cut to the 5-mm size and implanted on the cerebral cortex [33]. Briefly, PLGA and rGO were blended with 0.5-mL dimethyl sulfoxide and melted into a homogeneous mixture for extrusion-based 3D printing using the CELLINK BIO X6 printer. The scaffold was printed in 15 filament layers with approximately 80% porosity and in 5-mm (x-axis), 5-mm (y-axis), and 2-mm (z-axis) dimensions. After implantation, the area was covered with bone wax, and the scalp was closed with 4-0 absorbable surgical sutures (Ethicon, Inc). The rats recovered on a heating pad and were individually housed and monitored twice daily for the first 3 days, daily for 1 week, and weekly throughout the remaining 30-day study period. Buprenorphine was administered every 12 hours for 3 days after surgery, and ketoprofen (5 mg/kg) was administered every 24 hours for 3 days after surgery. Baytril (100 mg per 400 mL) mixed into water with flavored Gatorade was provided for 1 week after surgery.

Neurological Function Evaluation

Animal recovery and neurological function were evaluated for each rat on days 1, 2, 3, 7, 14, and 21 after surgery. A modified neurological severity score was used to assess the body weight, general condition, physical appearance, breathing, spontaneous behavior, handling reaction, wound healing, and neurological evaluation of each rat [11,34-36]. These behaviors were graded on a scale from 0 (normal) to 30 and above (severe) to determine any neurological deficits that occurred from the cranial intervention or material implantation.

IHC of Brain Tissue

At the 1-month end-of-study time point, the intact brain was removed as previously described and placed in 10% formalin [37,38]. The cerebellum was removed, and the brain was dissected down the midsagittal plane, dividing the left and right hemispheres of the cerebral cortex. Each half was paraffin embedded and longitudinally sectioned. Sections were deparaffinized, hydrated, unmasked, stained, and mounted as previously described [30]. One histology section from all specimens was stained with hematoxylin and eosin (H&E; Azer Scientific, Inc) for assessment of cellular detail, and one histology section from all specimens was stained with Prussian blue for assessment of hemosiderin deposition using a 30-minute stain with 1:1 hydrochloric acid and potassium ferrocyanide. IHC was performed on the remaining sections using glial fibrillary acidic protein (GFAP; 1:500), neuronal nuclei (NeuN; 1:500; Cell Signaling Technology, Inc), von Willebrand factor (vWF; 1:1000; Abcam), neurofilament light chain (NEFL; 1:20), ionized calcium-binding adapter molecule 1 (Iba1; 1:500), and CD68 (1:500). The secondary antibodies used were goat antirabbit immunoglobulin G horseradish peroxidase (1:500) and rabbit antimouse immunoglobulin G horseradish peroxidase (1:500; Abcam). Briefly, GFAP identifies astrocytes, NeuN identifies neurons, vWF identifies vascularization, NEFL identifies neural cytoskeleton structure, Iba1 identifies microglia, and CD68 identifies phagocytic activity [39-44]. Sections were imaged using a BZ-X Series all-in-one fluorescent microscope (Keyence Corporation) at 5X, 10X, 20X, and 40X magnification. The H&E sections were analyzed by a trained histologist. For each section, multiple images were taken along the length of the section with 20% overlap and stitched together to create a single image of the entire section. Scale

bars were added. ImageJ software was used to analyze the stitched images [45]. They were selected for optimal contrast (blue) and threshold (pixel intensity values ranged from 150 to 250). The nerve was isolated from the background and converted to a black-and-white image (black=stained tissue).

Statistical Analysis

For each section, the nerve was measured for percentage of area (percentage of black in the image) [30]. Mean and SD values were obtained. Prism (version 10; GraphPad Software) was used to perform a Shapiro-Wilk test of normality. When all data were determined to be normally distributed, *t* tests were performed for statistical significance between the control and injured tissues. Statistical significance was determined as a *P* value of .05 or less.

Results

A TBI is a complex disease in which a primary injury results in an immediate disruption of brain tissue caused by an external source, leading to contusion, hemorrhage, and axonal shearing. The secondary injury evolves over the following hours, days, and months, involving a cascade of degenerative molecular events leading to cell death [13,19]. Patients who experience focal, penetrating TBIs have areas of brain laceration, disruption of the leptomeninges, subdural hemorrhage, and cerebral edema [43]. Our method of injury manually disrupted the dura mater and cerebral cortex with a small blade through the cranial opening (Figure 1A). When the scaffold was placed onto the exposed brain tissue for rats 1, 2, and 4, there was minor bleeding before the scaffold was placed against the brain tissue with mild pressure. With rat 3, there was heavy bleeding after the surgical procedure, and the scaffold was placed onto the brain tissue after ensuring that the bleeding was under control. Evidence of the differences in the surgical implantation was observed 30 days later during the brain dissection. In rats 1, 2, and 4, the scaffold was more strongly incorporated into the surrounding bone of the craniotomy than into the brain tissue (Figure 1B). Some theories as to why this may have occurred include the location of the implanted material, which may not have been pushed sufficiently through the cranial opening; the large z-axis of the implanted scaffold possibly interfering with the implantation process; or excessive cerebral pressure or edema possibly pushing the construct back into the opening due to insufficient closing using the bone wax. Meanwhile, rat 3 showed a greater incorporation into the brain tissue (Figure 1C). This may be due to the more severe damage to the brain, evident in the heavy bleeding and deeper implantation of the scaffold.

Figure 1. (A) Image of the craniotomy location. (B) Brain dissection of rat 4 (tissue pen used to circle area of injury; black arrow indicates implanted material). (C) Brain dissection of rat 3 (deeper cortex injury and material implantation; black arrow indicates implanted material).

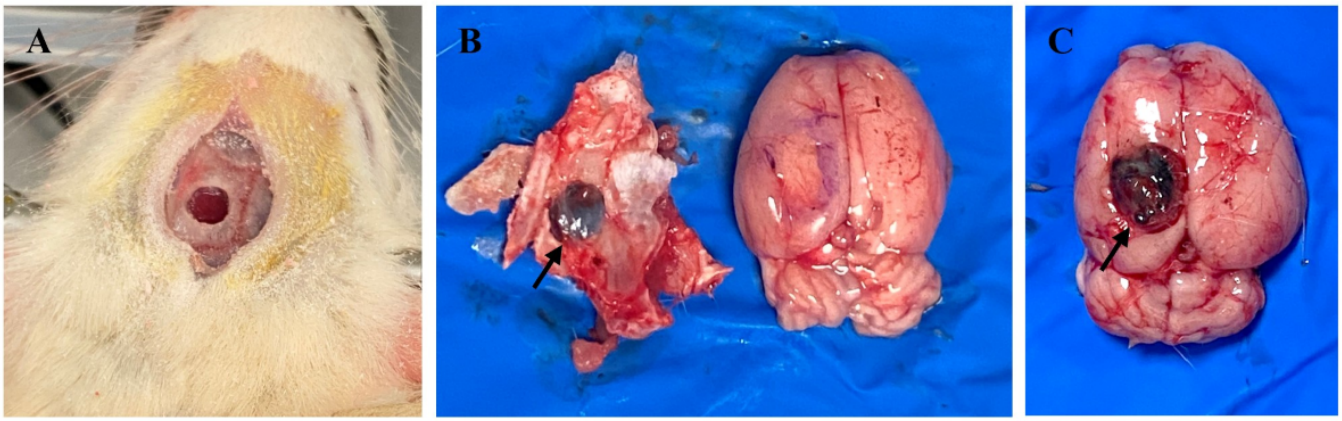

During the 30-day study, the neurological assessment evaluated the physical and behavioral changes that may occur with a TBI [11,34-36]. At the 6 time points, all rats showed no changes in any of the areas assessed (Table 1). Rat 3 took slightly longer to come out from anesthesia, which was expected due to the longer procedure time to control the heavy bleeding. However, while rat 3 showed slightly slower spontaneous movement, it still fell within normal parameters. While this indicated no immediate concerns regarding a foreign body rejection of the implanted PLGA and rGO scaffold, it also indicated that the TBI model may not have been severe enough to implicate neurological deficits common with the disease. Other than TBI severity, the points of neurological evaluation may be expanded to include additional behavior tests, identifying more minute behavioral changes in future studies. Monitoring of intracranial pressure throughout a future study may also aid in confirmation of a TBI as it is a signature symptom of the injury.

At the end of the 30-day study, H&E-stained sections were evaluated for local tissue reactions. Similar to the lateral fluid percussion injury model where the TBI is limited to 1 cerebral hemisphere, the contralateral side may be used as a comparison for neural injury [12,13]. As the injury was limited to the left cerebral cortex, the right cerebral cortex was used as uninjured control tissue. The H&E-stained tissue confirmed that no significant pathology was identified in the control tissues for all 4 rats (Figure 2A). For the injured side, rats 1, 2, and 4 showed a slight indentation to the cortex with mildly thickened leptomeninges, reactive small blood vessels, increased stromal cells, and hemosiderin deposition (Figures 2B and 2C). Hemosiderin deposition is a sign of

injury, often occurring after hemorrhage, and was confirmed via Prussian blue staining. Together, these findings indicate a mild focal cerebral meningeal fibrosis injury. This type of chronic response may occur after a penetrating TBI [46]. Rat 3 showed a cavitated region of the cerebrum where the meninges was severely expanded by a mass (Figures 2D-2F). The mass was composed of neutrophils and necrotic cell debris, marginated by histiocytic infiltrate, and a periphery of fibrovascular tissue with aggregated plasma cells, lymphocytes, and occasional multinucleate foreign body giant cells. Some of the rGO deposits in the area were associated with distinct vacuoles. Hemosiderin deposition was also evident and confirmed through Prussian blue staining. No evidence of infectious agents was present. Overall, rat 3 had evidence of severe focal chronic pyogranulomatous meningitis and a foreign body reaction to the rGO nanoparticles. It was difficult to decipher whether the injury was more severe in rat 3 or whether the strong inflammatory and immune response was solely due to the scaffold. Future studies will further investigate the separation in these data using a sham surgical group and an untreated TBI group.

Table 1. Neurological evaluation score sheet indicating the response of all rats at all time points throughout the 30-day study. Evaluation indicated no abnormal behavior or physical reactions after surgery, injury, and material implantation.

Evaluation domain and score scale	Rat 1	Rat 2	Rat 3	Rat 4
Loss of body weight				
<5% (0 points)	✓	✓	✓	✓
5%-10% (1 point)				
11%-15% (5 points)				
16%-20% (10 points)				
>20% (30 points)				
General condition and physical appearance				
Well-groomed, clean fur, clean and intact wound, and clear eyes (0 points)	✓	✓	✓	✓
Coat slightly unkempt and eye redness or “red tears” (chromodacryorrhea; 1 point)				
Coat dirty and shaggy, orbital tightening, nose flattening, ear and whisker changes, skin pinch (dehydration test), and some goosebumps (piloerection; 5 points)				
Coat unkempt and piloerection (10 points)				
Breathing				
Normal breathing (0 points)	✓	✓	✓	✓
Abnormally rapid breathing (tachypnea; 5 points)				
Difficult or labored breathing (dyspnea; 10 points)				
Spontaneous behavior				
Normal movements or locomotion (0 points)	✓	✓	✓	✓
Reluctance to move and slightly abnormal gait (5 points)				
Lethargic, apathetic, and abnormal gait (10 points)				
Significant mobility problems and mobility intermittent (<12 h; 20 points)				
Immobile for >12 h (30 points)				
Handling reaction				
Normal curiosity and alert (0 points)	✓	✓	✓	✓
Tense and nervous when held (5 points)				
Markedly distressed when handled (eg, shaking, vocalizing, and aggression; 10 points)				
Wound healing				
Wound clear, sutures and wound clip in place, and no signs of infection (0 points)	✓	✓	✓	✓
Wound closure insufficient, open wound, and no signs of infection (5 points)				
Wound showing initial signs of infection—swelling and redness (10 points)				
Wound infection severe—swelling, redness, and discharge (25 points)				
Neurological evaluation				
No observable deficit (0 points)	✓	✓	✓	✓
Forelimb flexion (paws pulled in when held by tail; 1 point)				
Decreased resistance to lateral push (slow, less movement, and pushback when the side is pushed)+forelimb flexion (5 points)				
Circling (circular movement when held by tail)+decreased lateral push and forelimb flexion (10 points)				
Seizure, coma, and complete paralysis (30 points)				

Evaluation domain and score scale	Rat 1	Rat 2	Rat 3	Rat 4
Total score				
Score of 0-9: minimal or no action required	✓	✓	✓	✓
Score of 10-20: provide supplementary care as needed				
Score of 21-29: consult veterinarian for additional care				
Score of ≥30: implement animal removal				

Figure 2. Hemoxylin and eosin–stained sections of brain tissue: (A) normal, healthy brain tissue on the control side at 40X magnification; (B) mild meningeal thickening and evidence of hemosiderin in rat 2 (injured side at 40X magnification); (C) brown and orange hemosiderin deposits and black graphene material deposits in rat 3 (injured side at 40X magnification); and images at 2X magnification (D), 10X magnification (E), and 40X magnification (F) exhibiting an abscess surrounding the graphene material implant in rat 3.

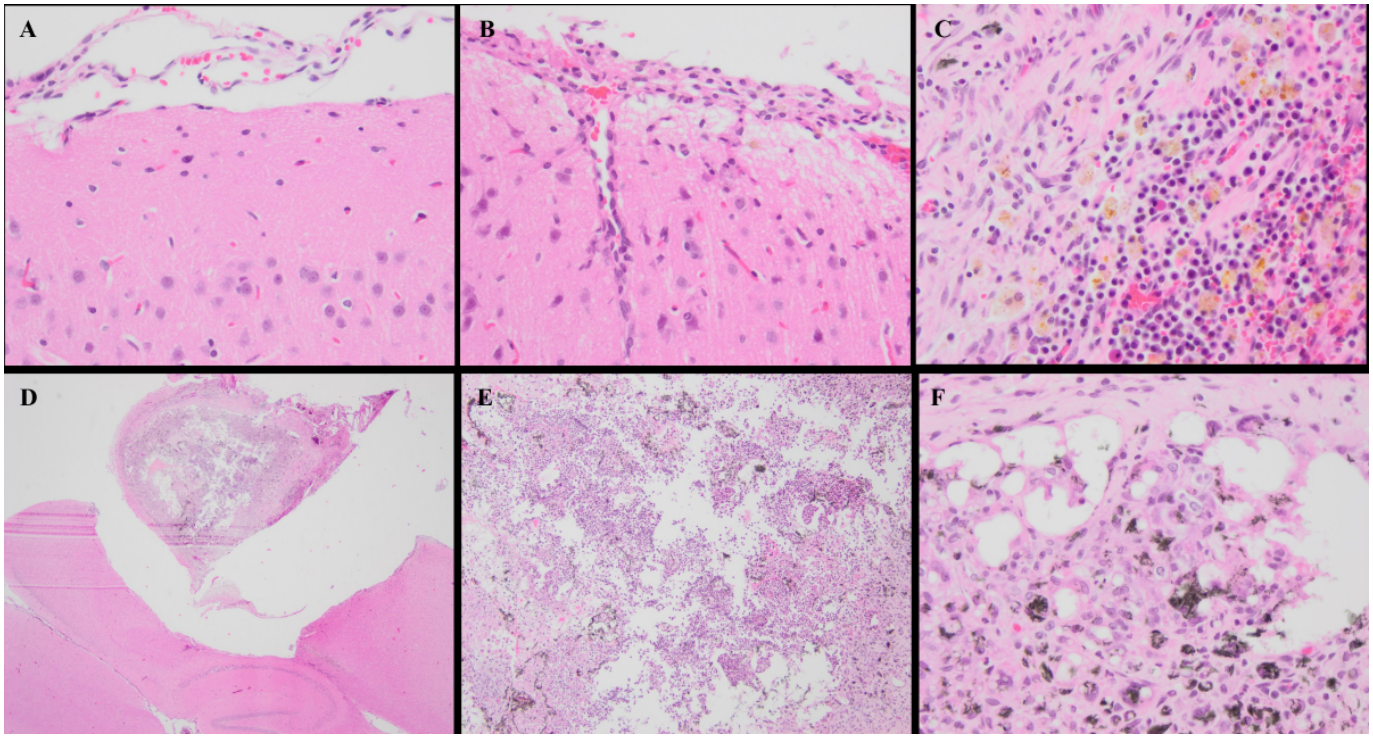

The IHC markers that were evaluated had previously shown changes after TBI. After an injury, the glial markers, GFAP and Iba1, increase, whereas the neural marker, NeuN, decreases due to glial scarring and the loss of damaged neural cells in the area, respectively [40,41,43]. vWF increases to identify vascular damage after a severe injury but typically maintains its expression with a mild injury [40]. NEFL increases to identify fragmented neural structures, and CD68 increases to indicate a rise in phagocytic activity [39,43]. Qualitatively, each of these 6 markers showed "normal" anatomical structures (Figures 3A-3F). Quantitatively, GFAP, vWF, NEFL, Iba1, and CD68 showed no significant differences in expression between the injured and control tissues (Figure 3G). However, NeuN expression significantly decreased from 9.65% to 4.56% of area stained in the injured tissue in all rats (P=.02). A significant decrease in NeuN is expected after a TBI, with the associated loss of neural cells due to the sustained damage to the tissue [40,43]. When rat 3 was excluded from the statistical analysis, statistical significance remained unchanged. The remaining markers may not have indicated any changes due to the 30-day time frame. It has been shown that these markers return to preinjury levels by 14 days after a TBI in mild cases [43,44].

Overall, all rats showed evidence of a TBI histologically at 30 days after surgery, although they were asymptomatic according to the neurological assessment. Rats 1, 2, and 4 showed evidence of a mild, focal, penetrating TBI according to the H&E staining and IHC marker (NeuN). Rat 3 showed evidence of foreign body rejection that could not be separated from evidence of a severe TBI.

Figure 3. Immunohistochemistry (IHC) of injured brain tissue. (A) Representative image of glial fibrillary acidic protein (GFAP) expression at 20X magnification (the black arrow indicates spindlelike astrocytes). (B) Representative image of neuronal nuclei (NeuN) expression at 20X magnification (the black arrow indicates hollowing of neurons). (C) Representative image of von Willebrand factor (vWF) expression at 20X magnification (the black arrow indicates a blood vessel). (D) Representative image of neurofilament light chain (NEFL) expression at 20X magnification (the black arrow indicates neurofilament alignment throughout the tissue). (E) Representative image of ionized calcium-binding adapter molecule 1 (Iba1) expression at 10X magnification (the black arrow indicates expression by spindlelike microglia). (F) Representative image of CD68 expression at 10X magnification (the black arrow indicates phagocytic activity around graphene material). (G) Quantification of IHC staining for each marker comparing the control ipsilateral cortex tissue to the injured cortex tissue. No significant changes were observed in GFAP, vWF, NEFL, Iba1, and CD68 expression. NeuN had a significant decrease in expression at 30 days after injury as compared to the control tissue. *$P \leq .05$.

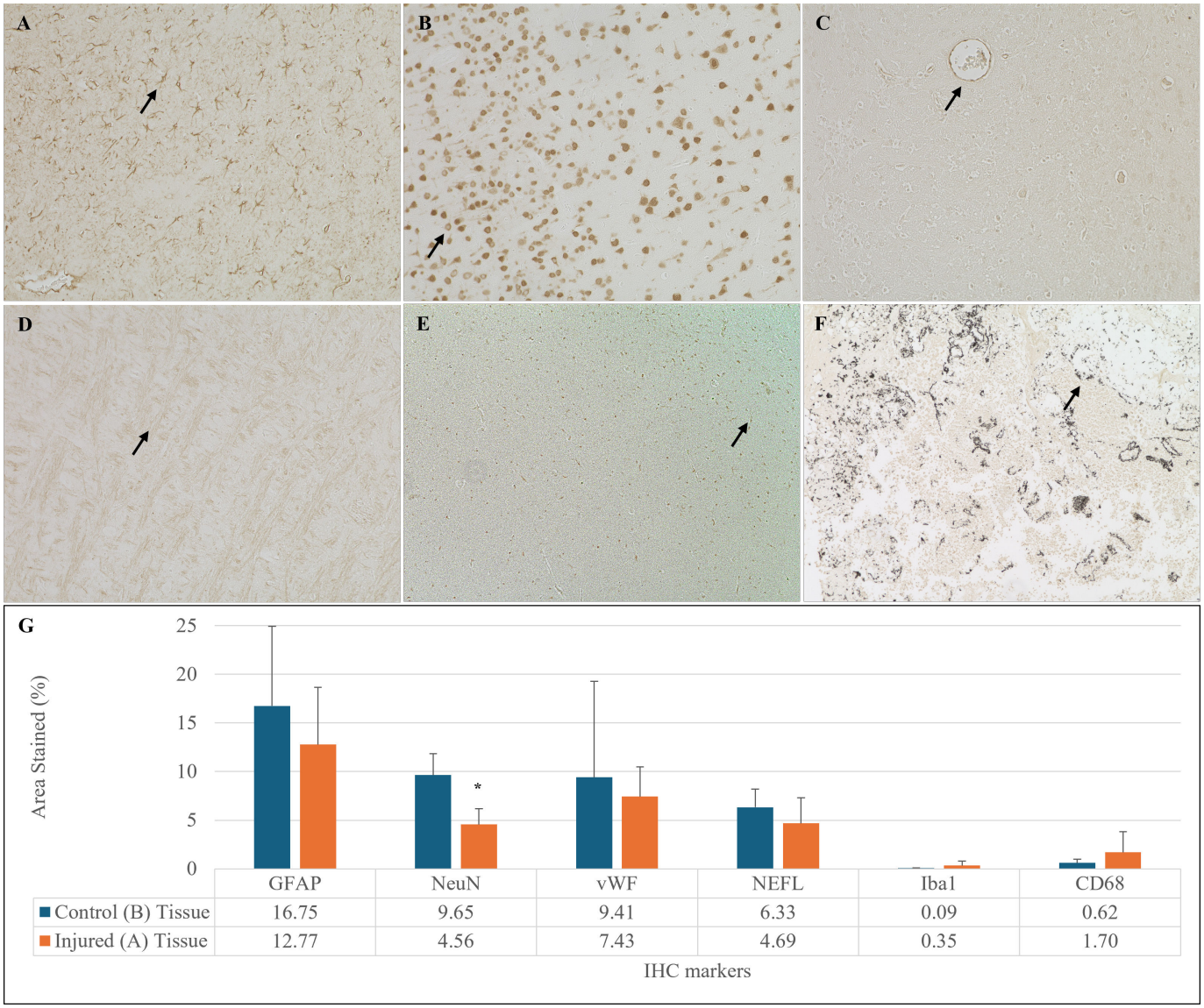

Discussion

Rat TBI models are diverse and designed to simulate human clinical scenarios and injuries. As a result, the models vary in their severity, location, and ease of animal handling [12]. As our goal in this study was to establish a tissue engineering strategy to address TBI, it required optimization at several steps. For instance, our strategy included selecting the animal in which to create the model; 3D printing the nanocomposite that we wanted to evaluate in vivo; establishing and optimizing procedures for implantation of the biomaterial; and, finally, validating protocols to monitor and evaluate the animals and assess the performance of the biomaterial scaffold. A pilot study of 4 Sprague Dawley rats was established and conducted as presented in this paper. We performed a relatively simple and quick craniotomy in rats to manually cut the BBB. The stereotaxic equipment was set to a consistent setting with respect to the cranial landmarks, allowing us to perform the surgery in a reproducible manner. Using our strategy, and as outlined in the Results section, we were able to prove the feasibility of this study, which allowed for scaffold implantation and in vivo safety evaluation of the biomaterial-tissue interaction. Finally, we were able to establish a scoring system to assess neurological features correlated with the defect. We created a neurological assessment based on published reports. We used histological and immunohistochemical staining to identify whether disruption of the BBB was sufficient to model a TBI, proving

that the novel biomaterial was biocompatible, and to evaluate the expression of specific neural target proteins to identify biomarkers for TBI for future studies.

Despite assessing only 4 rats in this study, we were able to validate our system, which could be applied to any future neural tissue engineering project focused on TBI. While this pilot study did not use a surgical control group, the use of a sham surgery in a larger study and with a greater number of animals for statistical analysis can separate the data to determine whether the injury identified through H&E staining was due to a severe TBI or to the implanted scaffold and whether the variability observed in 1 of the 4 rats evaluated was a concern in this model of TBI. Additionally, the surgical procedure was successful for scaffold implantation, although a construct with mechanical properties more aligned with those of the cortex will aid in the successful integration into the appropriate tissue [9,47,48]. A period of 30 days was chosen as this is the estimated time that a scaffold should remain implanted before degradation [49]. This time frame best allows for the alignment of complete degradation with tissue repair and regeneration in the cerebral cortex. The implanted scaffold did not fully degrade at 30 days in vivo and will need to be altered to accelerate degradation within this time frame. Future studies can evaluate the surgical groups at multiple time points, including a shorter time frame such as 24 hours or 3 days, to better confirm the acute injury (0-3 days) using TBI biomarkers such as those evaluated via IHC [19,43,44]. This will also allow for the evaluation of the therapeutic potential of implanted scaffolds and graphene nanoparticles at the acute and chronic TBI phases [9].

Acknowledgments

The authors acknowledge Matthew Cooper for the training on the stereotaxic surgical equipment.

Funding

This study was supported by departmental funds to the corresponding author (M Dhar). No external funding was used to support this study.

Data Availability

The datasets generated for this study are available from the corresponding author on reasonable request.

Authors' Contributions

MEH-T, M Dennis, and M Dhar were responsible for interpreting the data. MEH-T and M Dhar were responsible for conceptualizing the study and editing the manuscript. M Dennis and M Dhar were responsible for methodology. MEH-T was responsible for data acquisition and analysis, visualization, and initial manuscript preparation. M Dhar was responsible for supervision, resources, and writing review. All authors have read and agreed to the published version of the manuscript.

Conflicts of Interest

None declared.

References

1. Sulhan S, Lyon KA, Shapiro LA, Huang JH. Neuroinflammation and blood-brain barrier disruption following traumatic brain injury: pathophysiology and potential therapeutic targets. J Neurosci Res. Jan 2020;98(1):19-28. [doi: 10.1002/jnr.24331] [Medline: 30259550]
2. Vella MA, Crandall ML, Patel MB. Acute management of traumatic brain injury. Surg Clin North Am. Oct 2017;97(5):1015-1030. [doi: 10.1016/j.suc.2017.06.003] [Medline: 28958355]
3. D'Agostino R, Kursinskis A, Parikh P, Letarte P, Harmon L, Semon G. Management of penetrating traumatic brain injury: operative versus non-operative intervention. J Surg Res. Jan 2021;257:101-106. [doi: 10.1016/j.jss.2020.07.046] [Medline: 32818778]
4. Mansour A, Powla PP, Alvarado-Dyer R, et al. Comparative analysis of clinical severity and outcomes in penetrating versus blunt traumatic brain injury propensity matched cohorts. Neurotrauma Rep. 2024;5(1):348-358. [doi: 10.1089/neur.2024.0009] [Medline: 38595793]
5. Obukohwo OM, Oreoluwa OA, Andrew UO, Williams UE. Microglia-mediated neuroinflammation in traumatic brain injury: a review. Mol Biol Rep. Oct 19, 2024;51(1):1073. [doi: 10.1007/s11033-024-09995-4] [Medline: 39425760]
6. Basit RH, Wiseman J, Chowdhury F, Chari DM. Simulating traumatic brain injury *in vitro*: developing high throughput models to test biomaterial based therapies. Neural Regen Res. Feb 2023;18(2):289-292. [doi: 10.4103/1673-5374.346465] [Medline: 35900405]
7. Zhang J, Wang RJ, Chen M, et al. Collagen/heparan sulfate porous scaffolds loaded with neural stem cells improve neurological function in a rat model of traumatic brain injury. Neural Regen Res. Jun 2021;16(6):1068-1077. [doi: 10.4103/1673-5374.300458] [Medline: 33269752]
8. Galgano M, Toshkezi G, Qiu X, Russell T, Chin L, Zhao LR. Traumatic brain injury: current treatment strategies and future endeavors. Cell Transplant. Jul 2017;26(7):1118-1130. [doi: 10.1177/0963689717714102] [Medline: 28933211]

9. Aqel S, Al-Thani N, Haider MZ, et al. Biomaterials in traumatic brain injury: perspectives and challenges. Biology (Basel). Dec 29, 2023;13(1):21. [doi: 10.3390/biology13010021] [Medline: 38248452]
10. Ribitsch I, Baptista PM, Lange-Consiglio A, et al. Large animal models in regenerative medicine and tissue engineering: to do or not to do. Front Bioeng Biotechnol. 2020;8:972. [doi: 10.3389/fbioe.2020.00972] [Medline: 32903631]
11. Pinkernell S, Becker K, Lindauer U. Severity assessment and scoring for neurosurgical models in rodents. Lab Anim. Dec 2016;50(6):442-452. [doi: 10.1177/0023677216675010] [Medline: 27909194]
12. Fesharaki-Zadeh A, Datta D. An overview of preclinical models of traumatic brain injury (TBI): relevance to pathophysiological mechanisms. Front Cell Neurosci. 2024;18:1371213. [doi: 10.3389/fncel.2024.1371213] [Medline: 38682091]
13. Xiong Y, Mahmood A, Chopp M. Animal models of traumatic brain injury. Nat Rev Neurosci. Feb 2013;14(2):128-142. [doi: 10.1038/nrn3407] [Medline: 23329160]
14. Zhao Q, Zhang J, Li H, Li H, Xie F. Models of traumatic brain injury-highlights and drawbacks. Front Neurol. 2023;14:1151660. [doi: 10.3389/fneur.2023.1151660] [Medline: 37396767]
15. Graham NS, Sharp DJ. Understanding neurodegeneration after traumatic brain injury: from mechanisms to clinical trials in dementia. J Neurol Neurosurg Psychiatry. Nov 2019;90(11):1221-1233. [doi: 10.1136/jnnp-2017-317557] [Medline: 31542723]
16. Ławkowska K, Pokrywczyńska M, Koper K, Kluth LA, Drewa T, Adamowicz J. Application of graphene in tissue engineering of the nervous system. Int J Mol Sci. Dec 21, 2021;23(1):33. [doi: 10.3390/ijms23010033] [Medline: 35008456]
17. Hui Y, Yan Z, Yang H, Xu X, Yuan WE, Qian Y. Graphene family nanomaterials for STEM cell neurogenic differentiation and peripheral nerve regeneration. ACS Appl Bio Mater. Oct 17, 2022;5(10):4741-4759. [doi: 10.1021/acsabm.2c00663] [Medline: 36102324]
18. Silva M, Pinho IS, Covas JA, Alves NM, Paiva MC. 3D printing of graphene-based polymeric nanocomposites for biomedical applications. Funct Compos Mater. 2021;2(1):8. [doi: 10.1186/s42252-021-00020-6]
19. Harley-Troxell ME, Steiner R, Advincula RC, Anderson DE, Dhar M. Interactions of cells and biomaterials for nerve tissue engineering: polymers and fabrication. Polymers (Basel). Sep 7, 2023;15(18):3685. [doi: 10.3390/polym15183685] [Medline: 37765540]
20. Tang M, Song Q, Li N, Jiang Z, Huang R, Cheng G. Enhancement of electrical signaling in neural networks on graphene films. Biomaterials. Sep 2013;34(27):6402-6411. [doi: 10.1016/j.biomaterials.2013.05.024] [Medline: 23755830]
21. Aleemardani M, Zare P, Seifalian A, Bagher Z, Seifalian AM. Graphene-based materials prove to be a promising candidate for nerve regeneration following peripheral nerve injury. Biomedicines. Dec 30, 2021;10(1):73. [doi: 10.3390/biomedicines10010073] [Medline: 35052753]
22. Convertino D, Trincavelli ML, Giacomelli C, Marchetti L, Coletti C. Graphene-based nanomaterials for peripheral nerve regeneration. Front Bioeng Biotechnol. 2023;11:1306184. [doi: 10.3389/fbioe.2023.1306184] [Medline: 38164403]
23. Tupone MG, Panella G, d'Angelo M, et al. An update on graphene-based nanomaterials for neural growth and central nervous system regeneration. Int J Mol Sci. Dec 2, 2021;22(23):13047. [doi: 10.3390/ijms222313047] [Medline: 34884851]
24. MacDonald AF, Harley-Troxell ME, Newby SD, Dhar MS. 3D-printing graphene scaffolds for bone tissue engineering. Pharmaceutics. Aug 31, 2022;14(9):1834. [doi: 10.3390/pharmaceutics14091834] [Medline: 36145582]
25. Yunus MA, Ramli MM, Osman NH, Mohamed R. Stimulation of innate and adaptive immune cells with graphene oxide and reduced graphene oxide affect cancer progression. Arch Immunol Ther Exp (Warsz). Jul 29, 2021;69(1):20. [doi: 10.1007/s00005-021-00625-6] [Medline: 34327598]
26. Dudek I, Skoda M, Jarosz A, Szukiewicz D. The molecular influence of graphene and graphene oxide on the immune system under in vitro and in vivo conditions. Arch Immunol Ther Exp (Warsz). Jun 2016;64(3):195-215. [doi: 10.1007/s00005-015-0369-3] [Medline: 26502273]
27. Kenry, Lee WC, Loh KP, Lim CT. When stem cells meet graphene: Opportunities and challenges in regenerative medicine. Biomaterials. Feb 2018;155:236-250. [doi: 10.1016/j.biomaterials.2017.10.004] [Medline: 29195230]
28. Ema M, Gamo M, Honda K. A review of toxicity studies on graphene-based nanomaterials in laboratory animals. Regul Toxicol Pharmacol. Apr 2017;85:7-24. [doi: 10.1016/j.yrtph.2017.01.011] [Medline: 28161457]
29. Rhazouani A, Gamrani H, El Achaby M. Synthesis and toxicity of graphene oxide nanoparticles: a literature review of in vitro and in vivo studies. Biomed Res Int. 2021;2021:5518999. [doi: 10.1155/2021/5518999] [Medline: 34222470]
30. Harley-Troxell ME, Pedersen AP, Newby SD, et al. 3D-printed poly (lactic-co-glycolic acid) and graphene oxide nerve guidance conduit with mesenchymal stem cells for effective axon regeneration in a rat sciatic nerve defect model. Int J Nanomedicine. 2025;20(501241):3201-3217. [doi: 10.2147/IJN.S501241] [Medline: 40098718]

31. Mahmood A, Wu H, Qu C, et al. Suppression of neurocan and enhancement of axonal density in rats after treatment of traumatic brain injury with scaffolds impregnated with bone marrow stromal cells. J Neurosurg. May 2014;120(5):1147-1155. [doi: 10.3171/2013.12.JNS131362] [Medline: 24460490]
32. Yan F, Li M, Zhang HQ, et al. Collagen-chitosan scaffold impregnated with bone marrow mesenchymal stem cells for treatment of traumatic brain injury. Neural Regen Res. Oct 2019;14(10):1780-1786. [doi: 10.4103/1673-5374.257533] [Medline: 31169196]
33. MacDonald AF. Mesenchymal stem cell fate on carbon-based biomaterials: implications for bone regeneration and repair [PhD thesis]. University of Tennessee; 2022. URL: https://trace.tennessee.edu/entities/publication/36873230-ae48-423c-9e75-df44e7cb9545 [Accessed 2026-06-30]
34. Laboratory animal biomethodology workshops. McGill University. URL: https://www.mcgill.ca/cmarc/workshops [Accessed 2026-06-30]
35. Jeon H, Ai J, Sabri M, et al. Neurological and neurobehavioral assessment of experimental subarachnoid hemorrhage. BMC Neurosci. Aug 25, 2009;10:103. [doi: 10.1186/1471-2202-10-103] [Medline: 19706182]
36. Hao Q, Zheng J, Hu Y, Wang H. Bone marrow mesenchymal stem cells combined with Sox2 increase the functional recovery in rat with traumatic brain injury. Chin Neurosurg J. 2019;5:11. [doi: 10.1186/s41016-019-0158-7] [Medline: 32922911]
37. Brzica H, Abdullahi W, Reilly BG, Ronaldson PT. A simple and reproducible method to prepare membrane samples from freshly isolated rat brain microvessels. J Vis Exp. May 7, 2018(135):57698. [doi: 10.3791/57698] [Medline: 29782001]
38. Aboghazleh R, Boyajian SD, Atiyat A, Udwan M, Al-Helalat M, Al-Rashaideh R. Rodent brain extraction and dissection: a comprehensive approach. MethodsX. 2023;12:102516. [doi: 10.1016/j.mex.2023.102516] [Medline: 38162147]
39. Neri M, Frati A, Turillazzi E, et al. Immunohistochemical evaluation of aquaporin-4 and its correlation with CD68, IBA-1, HIF-1α, GFAP, and CD15 expressions in fatal traumatic brain injury. Int J Mol Sci. Nov 10, 2018;19(11):3544. [doi: 10.3390/ijms19113544] [Medline: 30423808]
40. Yip PK, Hasan S, Liu ZH, Uff CE. Characterisation of severe traumatic brain injury severity from fresh cerebral biopsy of living patients: an immunohistochemical study. Biomedicines. Feb 22, 2022;10(3):518. [doi: 10.3390/biomedicines10030518] [Medline: 35327320]
41. Kim HJ, Han SJ. A simple rat model of mild traumatic brain injury: a device to reproduce anatomical and neurological changes of mild traumatic brain injury. PeerJ. 2017;5:e2818. [doi: 10.7717/peerj.2818] [Medline: 28070456]
42. Clark DP, Perreau VM, Shultz SR, et al. Inflammation in traumatic brain injury: roles for toxic A1 astrocytes and microglial-astrocytic crosstalk. Neurochem Res. Jun 2019;44(6):1410-1424. [doi: 10.1007/s11064-019-02721-8] [Medline: 30661228]
43. Ţolescu RŞ, Zorilă MV, Kamal KC, et al. Histological and immunohistochemical study of brain damage in traumatic brain injuries in children, depending on the survival period. Rom J Morphol Embryol. 2022;63(1):169-179. [doi: 10.47162/RJME.63.1.18] [Medline: 36074681]
44. Wang ML, Yu MM, Yang DX, Liu YL, Wei XE, Li WB. Longitudinal microstructural changes in traumatic brain injury in rats: a diffusional kurtosis imaging, histology, and behavior study. AJNR Am J Neuroradiol. Sep 2018;39(9):1650-1656. [doi: 10.3174/ajnr.A5737] [Medline: 30049720]
45. Schindelin J, Arganda-Carreras I, Frise E, et al. Fiji: an open-source platform for biological-image analysis. Nat Methods. Jun 28, 2012;9(7):676-682. [doi: 10.1038/nmeth.2019] [Medline: 22743772]
46. Fehlberg CR, Lee JK. Fibrosis in the central nervous system: from the meninges to the vasculature. Cell Tissue Res. Mar 2022;387(3):351-360. [doi: 10.1007/s00441-021-03491-y] [Medline: 34189605]
47. Sensharma P, Madhumathi G, Jayant RD, Jaiswal AK. Biomaterials and cells for neural tissue engineering: current choices. Mater Sci Eng C Mater Biol Appl. Aug 1, 2017;77:1302-1315. [doi: 10.1016/j.msec.2017.03.264] [Medline: 28532008]
48. Cangellaris OV, Gillette MU. Biomaterials for enhancing neuronal repair. Front Mater. 2018;5. [doi: 10.3389/fmats.2018.00021]
49. Modo M. Bioscaffold-induced brain tissue regeneration. Front Neurosci. 2019;13:1156. [doi: 10.3389/fnins.2019.01156] [Medline: 31787865]

Abbreviations

BBB: blood-brain barrier
GFAP: glial fibrillary acidic protein
H&E: hematoxylin and eosin
Iba1: ionized calcium-binding adapter molecule 1

IHC: immunohistochemistry
NEFL: neurofilament light chain
NeuN: neuronal nuclei
PLGA: poly(lactic-co-glycolic) acid
rGO: reduced graphene oxide
TBI: traumatic brain injury
vWF: von Willebrand factor

Edited by Amy Schwartz; peer-reviewed by Firas Kobeissy; submitted 07.Apr.2025; final revised version received 13.May.2026; accepted 19.May.2026; published 10.Jul.2026

Please cite as:
Harley-Troxell ME, Dennis M, Dhar M
Material-Driven Therapeutics to Establish a Penetrating Traumatic Brain Injury Rat Model and Implantation of a 3D-Printed Scaffold: Pre-Experimental Pilot Study
JMIRx Bio 2026;4:e75613
URL: https://bio.jmirx.org/2026/1/e75613
doi: 10.2196/75613